Pramana – J. Phys., Vol. 39, No. 6, December 1992, pp. 639–653. © Printed in India.

Temperature dependent study of the single crystal electronic spectrum of octahedral Ni^{2+} ion subjected to distortions in weak fields

G V R CHANDRAMOULI and P T MANOHARAN
Department of Chemistry, Indian Institute of Technology, Madras 600036, India

MS received 31 March 1992; revised 17 July 1992

Abstract. Electronic spectra of two high spin d^8 nickel complexes, $Ni(en)_3Cl_2 \cdot 2H_2O$ and $Ni(OAc)_2 \cdot 4H_2O$, are reported. Polarized spectra were measured at 298 K. Temperature dependent spectra were measured using unpolarized light down to 20 K. The spectra at 20 K are well resolved revealing the features of spin-forbidden transitions and vibrational fine structure on some of the bands. Some of the spectra are deconvoluted to separate out the overlapping bands. The assignments are made using D_3 symmetry for $Ni(en)_3Cl_2 \cdot 2H_2O$ complex while D_4 symmetry is used for $Ni(OAc)_2 \cdot 4H_2O$. The energies of the spectroscopic states are calculated and compared with the observed transition energies. The distortion parameters are determined.

Keywords. Electronic spectrum; high spin; nickel ion; distorted octahedral symmetry.

PACS Nos 33·10; 33·20; 33·70

1. Introduction

The electronic spectrum of d^8 nickel complexes in weak ligand fields has been reported and reviewed by several authors in the past four decades (Jorgensen 1955; Pappalarado 1957; Holmes and McClure 1957; Liehr and Ballhausen 1959; Ballhausen and Liehr 1959; Piper and Koertge 1960; Ballhausen 1962, 1971; Balkanski *et al* 1964; Dingle and Palmer 1966; Perumareddi 1967, 1972; Narayana *et al* 1968). The expressions for interpretation of these spectra were given by pioneers in this field (Ballhausen and Liehr 1959; Perumareddi 1972). However, there are a few instances where incorrect interpretations were made due to insufficient resolution in the observed spectrum e.g. though the spectrum of $Ni(OAc)_2 \cdot 4H_2O$ was measured at 77 K, temperature dependent effects were not carefully noted down by the authors (Narayana *et al* 1968). In a similar system, $NiSO_4 \cdot 7H_2O$, which is also essentially oxygen coordinated, Holmes and McClure (1957) have demonstrated the importance of temperature dependent effects. In fact, a careful temperature dependent study down to 20 K on $Ni(OAc)_2 \cdot 4H_2O$ also yields well resolved spectrum revealing the features of spin-forbidden transitions. The crystal structure of this compound suggests a slight tetragonal distortion to the octahedral field (Van Niekerk and Schoening 1953). A comparative study of this system with a trigonal distortion which was well described by Dingle and Palmer (1966) leads to an accurate interpretation. For the sake of completeness we present here the electronic spectrum of trigonally distorted $Ni(en)_3Cl_2 \cdot 2H_2O$ instead of the spectrum of the $Ni(en)_3(NO_3)_2$ reported by Dingle and Palmer where the nitrate absorption masks some of the $d \rightarrow d$ transitions.

2. Experimental

The compound $Ni(en)_3Cl_2 \cdot 2H_2O$ was prepared by mixing a solution of nickel chloride in water and ethylenediamine in 1:3 molar proportions. Large diamond-shaped plate-like crystals of violet colour were obtained on slow evaporation of this solution. The crystals of nickel acetate tetrahydrate were grown on slow evaporation of a saturated solution in water. Emerald green prismatic crystals were obtained which contain a flat face and a long axis. The morphologies of both the crystals were determined using an Enraf-Nonius CAD-4 single crystal X-ray diffractometer. The flat face of the $Ni(en)_3Cl_2 \cdot 2H_2O$ crystal was found to be (010) and the *a*- and *c*-axes are oriented along the diagonals. In $Ni(OAc)_2 \cdot 4H_2O$ the long (needle) axis is found to be *a*-axis while the flat is $(0\bar{1}1)$. The spectral measurements were made using CARY-2390, Carl-Zeiss DMR-21 spectrophotometers and a microspectrophotometer developed in our laboratory for polarized optical spectral measurements in the UV–VIS region for small single crystals. The spectra presented in the figures were obtained from the former two instruments. The crystals were mounted on the cold head attached with a crystal mount of CTI cryogenics cryodyne cryocooler for temperature dependent measurements with CARY-2390 spectrophotometer. A liquid nitrogen cryostat was used for measurements on DMR-21 spectrophotometer. A pair of Glan prisms was used for polarization measurements. Polarized spectral measurements on ethylenediamine complex were made keeping the electric vector parallel and perpendicular to *a*-axis with light incident on *ac*-plane which is the flat face of the crystal. In the case of the acetate complex, the electric vector was oriented in parallel and perpendicular directions to the *a*-axis with light incident on $(0\bar{1}1)$ plane.

3. Crystal and molecular structures

Since crystal structure of $Ni(en)_3Cl_2 \cdot 2H_2O$ was not available, unit cell dimensions were determined using Enraf-Nonius CAD-4 single crystal X-ray diffractometer. This belongs to a monoclinic system with $a = 8{\cdot}730(6)$ Å, $b = 13{\cdot}90(8)$ Å, $c = 12{\cdot}9631(44)$ Å and $\beta = 93{\cdot}31°$. This is isomorphous with $Zn(en)_3Cl_2 \cdot 2H_2O$ whose crystal structure is known (Muralikrishna *et al* 1983). Hence the interpretations were made on the basis of the structure of the zinc complex. The molecular structure is shown in figure 1(a). The symmetry of the molecule is D_3. There are four molecules per unit cell whose molecular axes are oriented parallel to the *a*-axis of the crystal. Hence the measured polarizations correspond to the polarizations with respect to the molecular axes.

The crystals of $Ni(OAc)_2 \cdot 4H_2O$ belong to the monoclinic system $P2_1/c$ with two molecules per unit cell related to each other by a centre of inversion. The molecular structure is shown in figure 1(b). The NiO_6 moiety belongs to D_4 symmetry where the molecular axis is along one of the Ni–OH_2 bond directions rather than Ni–OAc bond. The Ni–O bond lengths (Van Niekerk and Schoening 1953): Ni–OAc = 2·12 Å, Ni–OH_2(1) = 2·11 Å and Ni–OH_2(2) = 2·06 Å indicate a tetragonal compression. Unlike ethylenediamine, the external morphology of this crystal is unfavourable for precise polarization measurements. The molecular axis makes an angle of 61° with *a*-axis while it makes 67° with the perpendicular to *a*-axis in $(0\bar{1}1)$. Hence very small

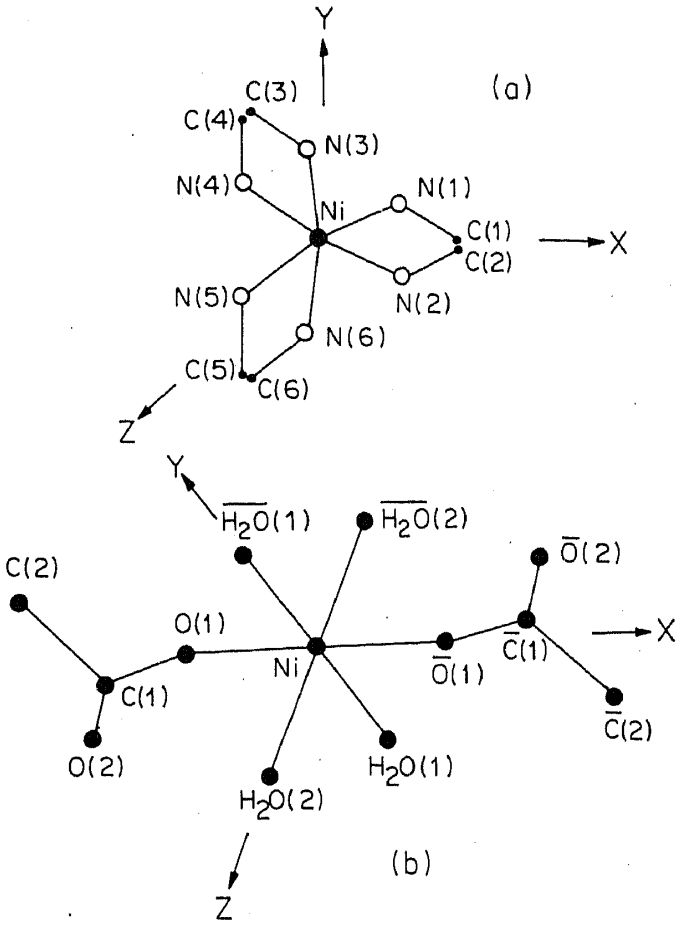

Figure 1. (a) Molecular structure of $Ni(en)_3$ moiety in $Ni(en)_3Cl_2 \cdot 2H_2O$. (b) Molecular structure of $Ni(OAc)_2 \cdot 4H_2O$.

differences were observed between parallel and perpendicular spectra. Though exact conclusions on polarizations of bands could not be drawn from these spectra, polarization are tentatively indicated.

4. Results

The polarized electronic spectrum of $Ni(en)_3Cl_2 \cdot 2H_2O$ measured parallel and perpendicular to *a*-axis in *ac* plane along with the unpolarized spectrum in the region 280–1200 nm is shown in figure 2. There are three broad absorptions in the range 8000–35000 cm^{-1}. A comparison of spectra recorded at 20 K and 300 K is shown in figure 3. Figures 2 and 3 reveal the complete shape of the high energy band. On cooling, a weak band at 34000 cm^{-1} appeared and picked up intensity till 20 K. The spin-forbidden transition centred at 21400 cm^{-1} was recorded at higher resolution which appears similar to the one reported earlier. The three broad band envelopes are observed in both parallel and perpendicular polarizations with differing intensity indicating that they contain multiple transitions of both polarization characteristics as described by Dingle and Palmer. Considering these factors, we have deconvoluted the entire spectrum (Barker and Fox 1980) both at 20 K and 300 K and the peak

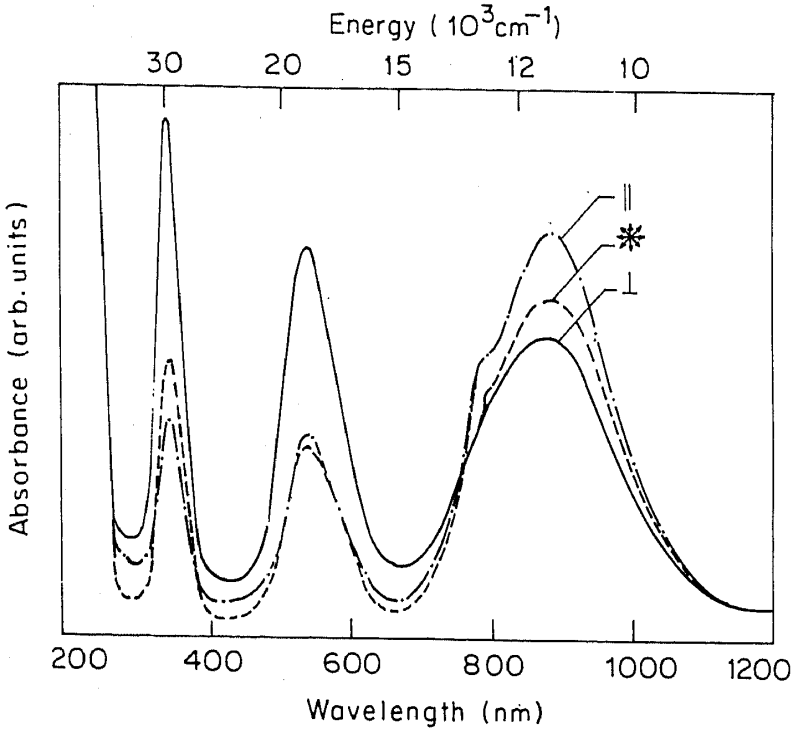

Figure 2. Single crystal electronic spectra of $Ni(en)_3Cl_2 \cdot 2H_2O$ at 300 K using polarized radiation with light incident on (010) plane keeping electric vector parallel (||), perpendicular (⊥) and using unpolarized radiation (✣).

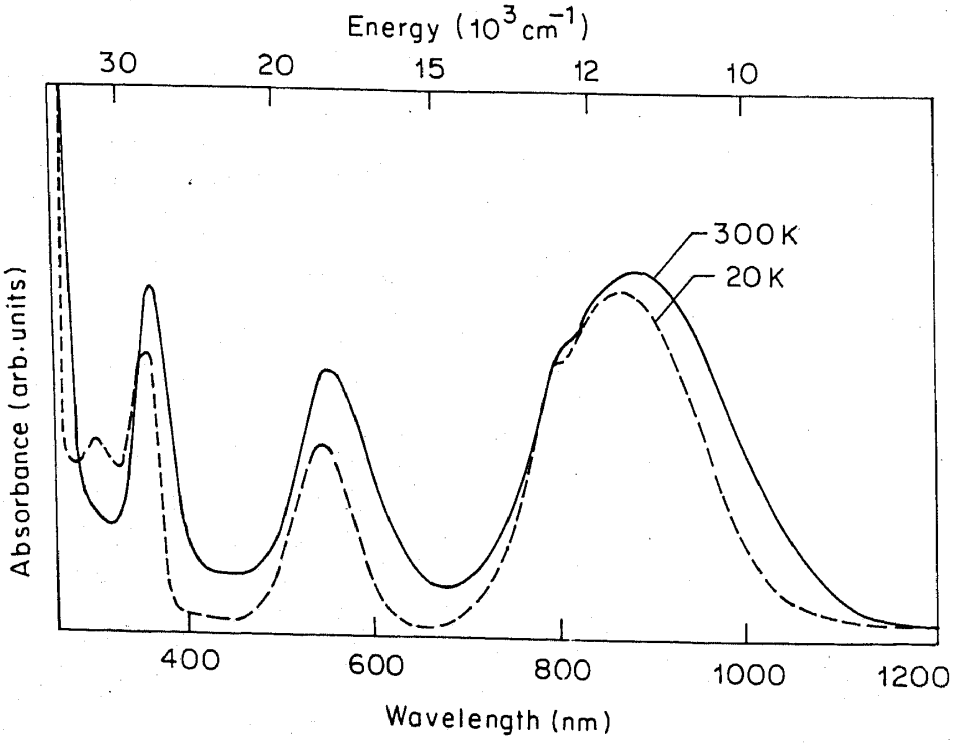

Figure 3. Single crystal electronic spectra of $Ni(en)_3Cl_2 \cdot 2H_2O$ at 20 K (---) and 300 K (———) using unpolarized radiation.

Table 1. Electronic spectrum of $Ni(en)_3Cl_2 \cdot 2H_2O$ at 300 K and their assignments under D_3 symmetry.

		300 K		20 K	
Excited[$] state	Polarization	Band maximum (cm^{-1})	Relative oscillator strength	Band maximum (cm^{-1})	Relative oscillator strength
$^3A_1[T_{2g}(F)]$	∥	10990	2·9	11270	2·2
$^3E[T_{2g}(F)]$	⊥	11780	6·2	11790	5·3
$^1E[D]$	⊥	12820	1·0	12640	1·1
$^3A_2[T_{1g}(F)]$	∥	18250	2·2	18390	1·1
$^3E[T_{1g}(F)]$	⊥	18580	6·3	18720	3·3
$^1A_1[G]$	⊥	21800	0·2	21400	0·2
$^1A_1[T_{2g}(D)]$	⊥	24260	1·1	24790	0·1
$^1E[T_{2g}(D)]$					
$^3A_2[T_{1g}(P)]$	∥	28570	5·2	28580	2·7
$^3E[T_{1g}(P)]$	⊥	29140	6·1	29580	4·0
$^1A_1[T_{2g}(G)]$	∥	33360	3·4	33110*	
$^1E[T_{2g}(G)]$			—	34840*	10·1
$^1E[E_g(G)]$				35970*	

*These three transitions which appear as one band in the observed spectrum were fitted to single Gaussian.
[$]Ground state is $^3A_2[^3A_{2g}(F)]$.

positions, polarizations and their relative oscillator strengths are given in table 1. The deconvoluted spectra at 20 K and 300 K are shown in figure 4.

The electronic spectrum of nickel acetate tetrahydrate crystals appears mainly as three broad band systems centred at 8470, 15600 and 25970 cm^{-1}. The polarized spectra in the region 300–800 nm at 298 K and 800–1600 nm at 77 K are shown in figure 5 and the temperature-dependent spectra from 18–275 K in the entire spectral region are shown in figures 6 and 7. From figure 5 it is clear that the band at 8470 cm^{-1} is a combination of at least two broad absorptions centred at 8470 and 9480 cm^{-1}. There is a gradual decrease in the intensity in the spectral region 1040–1480 nm as the temperature is lowered, indicating that the band at 8470 cm^{-1} is of vibronic origin. The intensity of the band at 9480 cm^{-1} remains the same at all temperatures except for a little blue shift. The second band system centred at 15600 cm^{-1} shows fine structure on cooling the crystal to 18 K. It is mainly composed of three bands centred at 13960, 15600 and 18400 cm^{-1}. A comparison of the spectra at various temperatures reveals that there is considerable decrease in the intensity of the broad band at 13960 cm^{-1}. The band centred at 15600 cm^{-1} reveals fine structure with spacings of 400–500 cm^{-1}. The peak height of the broad low intensity band centred at 18400 cm^{-1} slightly increases as the temperature is reduced, showing its possible orbital allowedness. A closer look reveals fine structure on this. The separation is found to be about 420 cm^{-1}. The third band system contains bands around 22940, 25970 and 28570 cm^{-1}. The low intensity broad absorption centred at 22940 cm^{-1} gradually decreases in intensity and it splits into two bands centred at 21650 and 22940 cm^{-1}. The band at 25970 cm^{-1} also decreases in intensity indicating its forbidden nature. A closer look into the variation of the shape of this band with temperature reveals that there is a band at 28570 cm^{-1} whose intensity

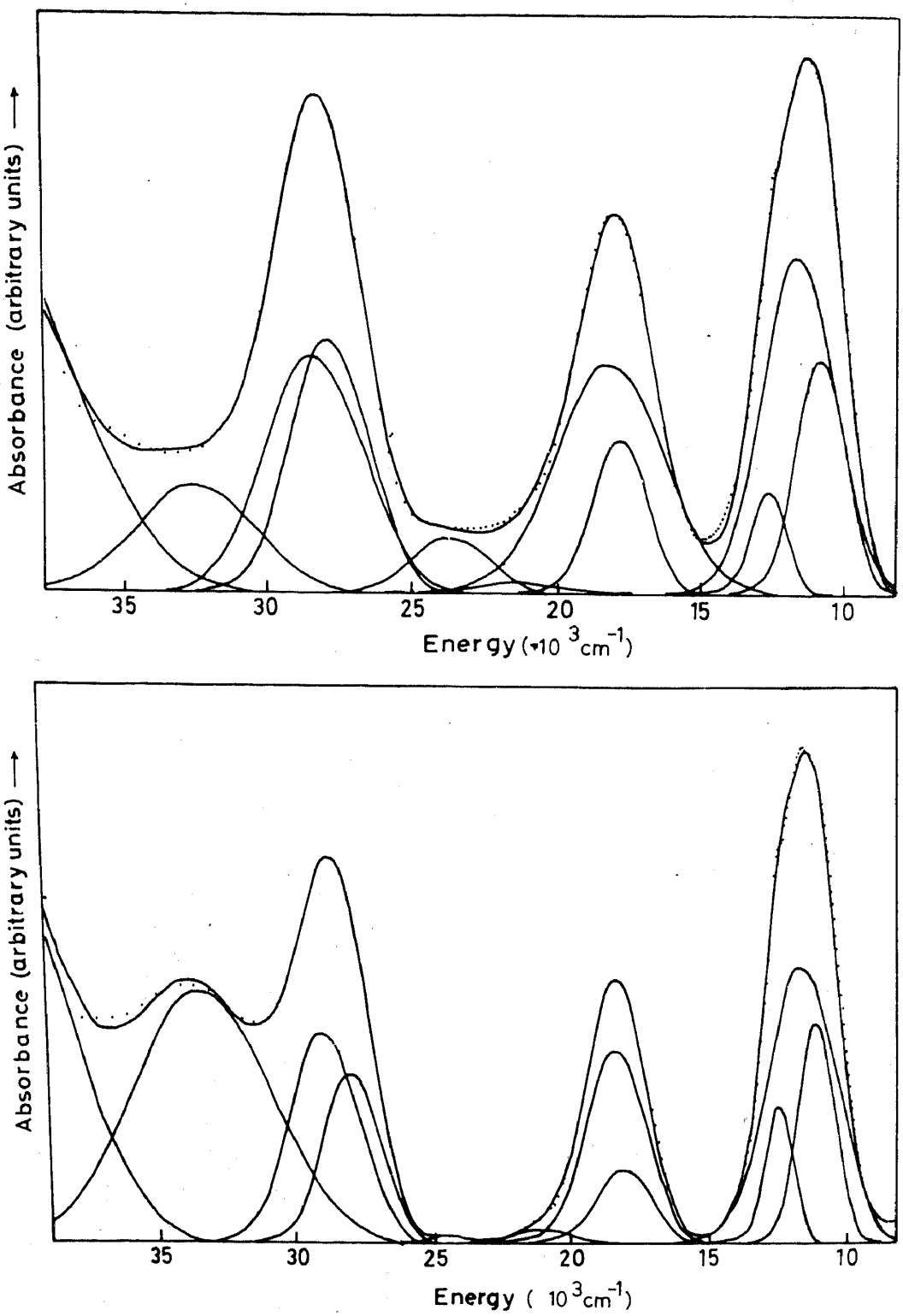

Figure 4. Deconvolution of electronic spectrum of $Ni(en)_3Cl_2 \cdot 2H_2O$ at 300 K (top) at 20 K (bottom) (——— fitted spectrum; ···· observed spectrum).

remains unchanged as the temperature is reduced. Finally the band in the region 35000 cm^{-1} gradually picks up intensity as the temperature is lowered and at 20 K it splits into two bands centred at 32680 and 34970 cm^{-1}. The increase in the intensity of these bands proves their allowed nature. All the band positions and splittings are

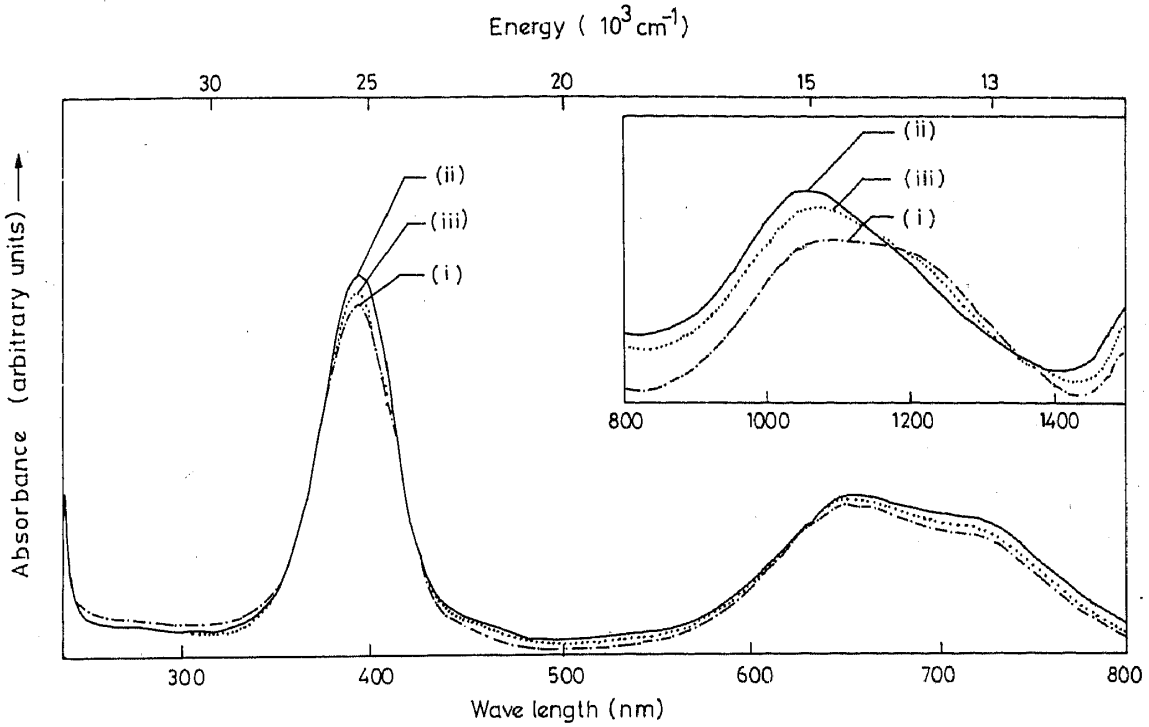

Figure 5. Single crystal electronic spectra of $Ni(OAc)_2 \cdot 4H_2O$ with light incident on (011) plane (i) parallel to *a*-axis (ii) perpendicular to *a*-axis and (iii) using unpolarized light. Inset shows the spectrum of infrared band at 77 K.

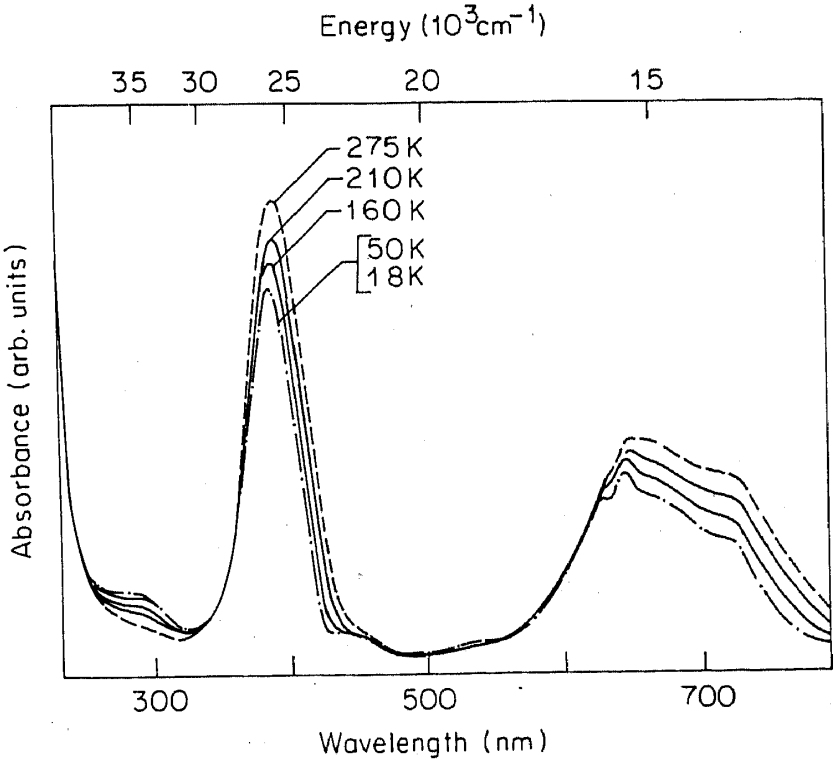

Figure 6. Temperature dependence of the electronic spectrum of single crystal of $Ni(OAc)_2 \cdot 4H_2O$ in the region 240–800 nm.

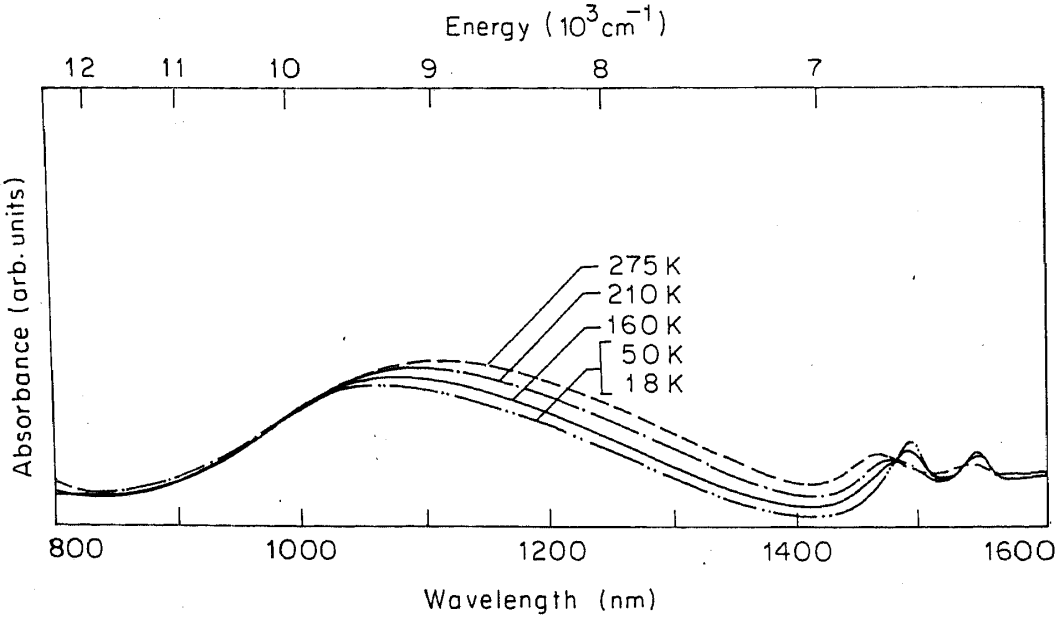

Figure 7. Temperature dependence of the electronic spectrum of single crystal of $Ni(OAc)_2 \cdot 4H_2O$ in the region 800–1600 nm.

given in table 2. A comparison of this spectrum with that of ethylenediamine complex reveals that there is one-to-one correlation of the bands in their number and intensity-gaining mechanism.

Though it is not in the scope of the present work, it is interesting to note that the band at 6810 cm^{-1} gradually decreases in intensity and shifts to lower energy on cooling down to 200 K and then picks up intensity maintaining the low energy shift on further cooling until 18 K. The absorption maximum has finally reached 6690 cm^{-1}. An isobestic point is noted at 6760 cm^{-1}. A similar band observed at 6480 cm^{-1} gradually increases in intensity with no accompanying energy shift as the temperature is lowered.

5. Discussion

5.1 $Ni(en)_3Cl_2 \cdot 2H_2O$

There is a general agreement between our results on $Ni(en)_3Cl_2 \cdot 2H_2O$ and those on $Ni(en)_3(NO_3)_2$ by Dingle and Palmer (1966) except for some new observations and a few differences. In accordance with the results of Dingle and Palmer, it is obvious that there has been a lowering of symmetry from pure octahedron of nitrogen ligands to D_3. Hence, the energy level scheme of octahedral Ni(II) complex (Dingle and Palmer 1966) has to be further split as shown below:

O_h	D_3
A_{1g}	A_1
A_{2g}	A_2
T_{1g}	$A_2 + E$
T_{2g}	$A_1 + E$

Table 2. Electronic spectrum of nickel acetate tetrahydrate.

Excited state	Polarization	Band maximum (cm^{-1}) 300 K	18 K	Calculated* transition energy
			6480	
			6690	
			6810	
$^3B_2[T_{2g}(F)]$	∥	8480	8470	8470
$^3E[T_{2g}(F)]$	⊥	9430	9480	9480
$^1B_1[E_g(F)]$	⊥			13290
$^3A_2[T_{1g}(F)]$	⊥	13890	13960	14140
		14990	14750	
		15350	15080	
$^3E[T_{1g}(F)]$	⊥	15760	15600	15250
			16000	
			16420	
			16810	
			17210	
$^1A_1[E_g(D)]$				16570
$^1E[T_{2g}(D)]$	⊥	17600	18400	21120
			18810	
			19230	
			19660	
$^1B_2[T_{2g}(D)]$	⊥	22220	21650	21640
$^1A_1[A_{1g}(G)]$	⊥		22940	23360
$^3A_2[T_{1g}(P)]$		25450		25970
$^3E[T_{1g}(P)]$	⊥		25970	26080
$^1E[T_{2g}(G)]$	⊥	28030	28570	27960
$^1A_1[E_g(G)]$				30520
$^1B_2[T_{2g}(G)]$	∥	34720	32680	34310
$^1B_1[E_g(G)]$			34970	34800

*Ground state is $^3B_1[A_{2g}(F)]$.
Calculated energies are obtained using $Dq = -847\,cm^{-1}$, $Ds = -550\,cm^{-1}$, $Dt = +115\,cm^{-1}$, $B = 900\,cm^{-1}$ and $C = 3500\,cm^{-1}$ in the expressions given in table 3.

In D_3 point group the electric dipole selection rules are

$A_2 \rightarrow A_2$ forbidden,

$A_2 \rightarrow A_1$ allowed, z polarized (∥),

$A_2 \rightarrow E$ allowed, xy polarized (⊥).

The electronic spectrum of $Ni(en)_3Cl_2 \cdot 2H_2O$ appears as three band structure as expected for a d^8 Ni(II) ion due to spin-allowed transitions in octahedral ligand field. In addition, there are a few low intensity spin-forbidden transitions.

5.1.1 *Spin-allowed transitions*: The assignments given by Dingle and Palmer completely hold good for the first band of our system also, except that we have deconvoluted it into three-component bands, the positions and assignments of which are found in table 1. However, an analysis of second band system based on the

temperature variation studies exhibits some interesting features. The peak observed at 18520 cm^{-1} shifts by about 460 cm^{-1} towards high energy region and its intensity decreases rapidly as the temperature is lowered. Dingle and Palmer assigned this broad band as a combination band whose assignment was given as

$$^3A_2 \rightarrow {}^3A_2[T_{1g}(F)] \text{ and } {}^3A_2 \rightarrow {}^3E[T_{1g}(F)].$$

By deconvolution we obtained the energy of first transition at 18390 cm^{-1} which is an orbitally forbidden transition and second transition at 18720 cm^{-1} which is the allowed component and $\perp$ polarized. The former transition may be allowed due to vibronic interaction of a vibronic mode α_2 or ε. The observed band intensity in parallel polarization cannot be explained if only $^3A_2 \rightarrow {}^3E$ is active. A transition $^3A_2 \rightarrow {}^3A_2\alpha_2$ will give rise to the observed parallel intensity. On the other hand, the peak shift and the temperature dependence of the band intensity also can be explained as a result of the contribution of this component band to the total band intensity. A fitting of the intensity of this transition with temperature using the formulation (Holmes and Mclure) $f = f_0(1 + e^{-1.44\omega/T})$, (where f is the f-number which is proportional to the oscillator strength at temperature T, f_0 is f-number at 0 K and ω is the frequency of the vibronic mode of the ground state) results in a frequency of 275 cm^{-1} for the enabling vibration α_2.

The broad band system centred at 29,580 cm^{-1} also shows similar behaviour. It shows a peak shift of 620 cm^{-1} towards high energy region with an overall reduction of intensity as the crystal was cooled down to 20 K. It is worth mentioning that this is again a combination band assigned by Dingle and Palmer as due to the transitions

$$^3A_2 \rightarrow {}^3A_2[T_{1g}(P)] \text{ and } {}^3A_2 \rightarrow {}^3E[T_{1g}(P)].$$

Furthermore, the absence of optical excitation due to NO_3^- ion in our system makes it easier to observe the shift and polarization of the band and identify the exact energy of excitation. It is interesting to observe that both the transitions $^3A_2$ to $^3T_{1g}$ of P and F exhibit similar polarizations and temperature dependence as expected. An analysis of temperature dependence of the band intensity revealed that the same α_2 vibronic mode enables the forbidden components of both the transitions.

5.1.2 *Spin-forbidden transitions*: The spin-forbidden transitions are observed at the energies 21400, 24790, 33110, 34840 and 35970 cm^{-1}. The transition at 21400 cm^{-1} showed vibronic fine structure at 20 K. This is assigned to $^3A_2 \rightarrow {}^1A_1[A_{1g}(G)]$. A complete discussion of the origin of the intensity and assignments of the fine structure are given by Dingle and Palmer (1966). The transition observed at 24790 cm^{-1} with a general $\perp$ polarization may be assigned as $^3A_2 \rightarrow {}^1A_1[T_{2g}(D)]$ and $^3A_2 \rightarrow {}^1E_1[T_{2g}(D)]$. The group of transitions observed in the region 33000–36000 cm^{-1} were not observed in the nitrate complex due to the absorption of nitrate ion. These are assigned as $^3A_2 \rightarrow {}^1A_1[T_{2g}(G)]$, $^3A_2 \rightarrow {}^1E_1[T_{2g}(G)]$ and $^3A_2 \rightarrow {}^1E[E(G)]$ on the basis of crystal field and electron repulsion parameters computed.

The trigonal distortion parameters were estimated using the energy expressions given by Perumareddi (1972) for d^8 nickel under trigonal distortion. The best fit of calculated transition energies with observed energies was obtained with the Racah parameters $B = 810\ cm^{-1}$ and $C = 4B$, crystal field splitting parameter $Dq = +1177\ cm^{-1}$, trigonal distortion parameters $D_\sigma = -250\ cm^{-1}$ and $D_\tau = -125\ cm^{-1}$ and spin-orbit coupling constant $\lambda = -275\ cm^{-1}$.

5.2 $Ni(OAc)_2 \cdot 4H_2O$

Temperature dependent optical spectra and polarization indicate a similarity between $[Ni(en)_3]^{2+}$ and $Ni(OAc)_2 \cdot 4H_2O$. Both these complexes show three band systems with low intensity spin-forbidden transitions. Ethylenediamine provides a stronger crystalline field than acetate and water. The symmetry is D_3 in the former complex while it is D_4 in the latter. The lowered symmetry from octahedral to D_4 in the latter compound rather than D_{4h} is justified by the identification of allowed nature of some of the $d \rightarrow d$ transitions in temperature-dependent studies. The energy levels under O_h point group split further in D_4 as shown below:

O_h	D_4
A_{1g}	A_1
A_{2g}	B_1
E_g	$A_1 + B_1$
T_{1g}	$A_2 + E$
T_{2g}	$B_2 + E$

The configuration d^8 gives rise to the Russell Saunder's terms of which ^3F and ^3P are of high spin multiplicity and ^1D, ^1G and ^1S are of low spin multiplicity. These terms again split by the perturbation of crystal field. The splitting of all these levels and their calculated energies using crystal field parameters $Dq = +847\,cm^{-1}$, $Ds = -550\,cm^{-1}$, $Dt = 115\,cm^{-1}$ and Racah parameters $B = 900\,cm^{-1}$ and $C = 3500\,cm^{-1}$ are given in table 2. The determinants to account for configuration interaction of the same symmetry states are presented in table 3. Spin-orbit coupling may also perturb the energy levels. This is demonstrated by Liehr and Ballhausen (1959) in the case of hydrates of Ni(II) ion. At a later stage a full calculation of the matrix elements including spin-orbit coupling and tetragonal distortions was presented by Perumareddi (1972). The parameters B, C, Dq, Ds, Dt and ξ were fitted by a least squares procedure in order to obtain best fit of the calculated energies with the experimentally observed transition energies. This leads to the values of the parameters as $B = 850\,cm^{-1}$, $C = 3400\,cm^{-1}$, $Dq = -858\,cm^{-1}$, $Ds = -360\,cm^{-1}$ and $Dt = -115\,cm^{-1}$, $\xi = -550\,cm^{-1}$. This calculation leads to thirty five states. Since the experimental spectrum could resolve only twelve transitions and the splittings due to spin-orbit coupling are not well resolved, we limit ourselves to assign the transitions on the basis of symmetry effects only.

The selection rules for electric dipole induced transitions in D_4 point group are:

$B_1 \rightarrow A_1, A_2, B_1$	forbidden
$B_1 \rightarrow B_2$	allowed, z-polarized
$B_1 \rightarrow E$	allowed, xy-polarized.

The first band system contains two broad bands centred at $8470\,cm^{-1}$ and $9480\,cm^{-1}$, the former being $\parallel$ polarized and the later $\perp$ polarized. Hence the former transition is assigned to $^3B_1 \rightarrow {}^3B_2[T_{2g}(F)]$. The transition at $9480\,cm^{-1}$ may be assigned as $^3B_1 \rightarrow {}^3E[T_{2g}(F)]$. The observed allowedness and the polarization of this

Table 3. Energy expressions for nickel acetate tetrahydrate.

$^3B_1[A_{2g}(F)]$ $\lvert -12Dq-7Dt-E\rvert=0$	$^3B_2[T_{2g}(F)]$ $\lvert -2Dq-7Dt-E\rvert=0$	
$^3E[T_{2g}(F)]$ $\lvert -2Dq+(7/4)Dt-E\rvert=0$		
$^3A_2[T_{1g}(F)]$ $\lvert 6Dq-(4/5)Ds+6Dt-E$	$^3A_2[T_{1g}(P)]$ $-4Dq+(12/5)Ds-4Dt$ $15B+(14/5)Ds-E\rvert=0$	
$^3E[T_{1g}(F)]$ $\lvert 6Dq-(2/5)Ds+(9/4)Dt-E$	$^3E[T_{1g}(P)]$ $-4Dq+(6/5)Ds-(3/2)Dt$ $15B-(7/5)Ds-E)\rvert=0$	
$^1B_2[T_{2g}(D)]$ $\lvert(16/7)Dq-(6/7)Ds+(4/7)Dt-E$	$^1B_2[T_{2g}(D)]$ $(\sqrt{3}/7)(-19Dq+4Ds-30Dt)$ $7B+(26/7)Dq-(8/7)Ds+(11/7)Dt-E\rvert=0$	
$^1E[T_{2g}(D)]$ $\lvert(16/7)Dq+(3/7)Ds+(16/7)Dt-E$	$^1E[T_{2g}(G)]$ $-(16\sqrt{3}/7)Dq$ $7B+(26/7)Dq-(4/7)Ds+(69/28)Dt-E\rvert=0$	
$^1B_1[E_g(D)]$ $\lvert(-24/7)Dq-(6/7)Ds-(4/7)Dt-E$	$^1B_1[E_g(G)]$ $-(\sqrt{3}/7)(-40Dq+4Ds-30Dt)$ $7B-(4/7)Dq-(8/7)Ds+(11/7)Dt-E\rvert=0$	
$^1A_1[E_g(D)]$ $\lvert(-24/7)Dq+(6/7)Ds-(24/7)Dt-E$	$^1A_1[G]$ $(1/\sqrt{105})(-26Dq+10Ds+51Dt)$ $7B-4Dq-(7/3)Dt-E$	$^1A_1[E_g(G)]$ $(-1/7\sqrt{3})(-52Dq+12Ds+21Dt)$ $(-1/3\sqrt{35})(60Ds+5Dt)$ $7B-(4/7)Dq+(8/7)Ds+(47/21)Dt-E\rvert=0$
$^1A_2[T_{1g}(G)]$ $\lvert -2Dq+4Ds-2Dt-E\rvert=0$	$^1E[T_{1g}(G)]$ $\lvert -2Dq-2Ds-(3/4)Dt-E\rvert=0$	

band confirm this assignment. The calculated energy of the transition $^3B_1 \rightarrow {}^1B_1[E_g(F)]$ is 13290 cm^{-1}. Probably this band is buried under the broad envelope of the above two bands since it is a low intensity spin-forbidden transition.

The second band system which appears in the region 13900–23000 cm^{-1} contains four bands. The band at 13960 cm^{-1} is $\perp$ polarized and is assigned to $^3B_1 \rightarrow {}^3A_2[A_{1g}(F)]$. This is in good agreement with the calculated transition energy 14140 cm^{-1}. This orbitally forbidden transition may have been allowed by an enabling vibrational species ε, which probably explains the observed $\perp$ polarization though no direct proof is available. The transition at 15600 cm^{-1} may be assigned as $^3B_1 \rightarrow {}^3E[T_{1g}(F)]$ which explains orbitally allowed nature of this band as well as its $\perp$ polarization. The fine structure observed on this band may be a vibrational progression with Ni–OH_2 stretching frequencies. It could also be interpreted as splitting due to spin-orbit coupling, since the band is itself of allowed nature. The calculation including spin-orbit coupling gives seven transitions under $^3T_{1g}$ at the energies 14470, 14530, 14750, 15630, 15640, 15830 and 15960 cm^{-1}. However, the observed spectrum shows approximately equal spacings of the fine structure and hence the fine structure should be assigned to vibronic progression rather than spin-orbit splittings.

The low intensity transition at 18400 cm^{-1} was not observed by the earlier workers. We assign it as due to $^3B_1 \rightarrow {}^1E[T_{2g}(D)]$ though its calculated energy including spin-orbit coupling or without it is approximately 21000 cm^{-1}. We have given this assignment since there is no other level nearby the energy 18400 cm^{-1}. This transition gains intensity under spin-orbit coupling term in the Hamiltonian with the nearby spin-allowed term. This is of course true, no matter whether the transition is electric or magnetic dipole allowed. It is also appropriate to mention here that, Piper and Koertge (1960) found in $Ni(H_2O)_6^{2+}$ a similar band, due to simultaneous electronic and vibrational excitations involving O–H stretching vibration. Part of the intensity of this band might have been drawn from similar mechanism. The two transitions at 21650 and 22940 cm^{-1} gain intensity by spin-orbit coupling. These are assigned to $^3B_1 \rightarrow {}^1B_2[T_{2g}(D)]$ and $^3B_1 \rightarrow {}^1A_1[G]$ respectively.

The third band system is composed of bands at 25970 and 28570 cm^{-1}. A careful observation of temperature dependence of the centre of first band reveals that the band centre has shifted by about 520 cm^{-1} on cooling down to 20 K. The calculated transition energies for $^3B_1 \rightarrow {}^3A_2[T_{1g}(P)]$ and $^3B_1 \rightarrow {}^3E[T_{1g}(P)]$ are 25970 and 26080 cm^{-1} respectively. This indicates that it is a combination of the above two transitions. The observed shift of the peak centre justifies the reduction in the intensity of the low energy component due to its orbital-forbidden nature. The band at 28570 cm^{-1} is assigned to a spin-forbidden transition $^3B_1 \rightarrow {}^1E[T_{2g}(G)]$. The spin-forbidden transition around 34000 cm^{-1} is well resolved at 20 K showing up its components centred at 32680 cm^{-1} and 34970 cm^{-1}. These transitions can be assigned as $^3B_1 \rightarrow {}^1B_2[T_{2g}(G)]$ and $^3B_1 \rightarrow {}^1B_1[E_g(G)]$ respectively. The infrared bands at 6480, 6690 and 6810 cm^{-1} are possibly the overtone frequencies of water. Their intensity variations with temperature probably indicate the changes in their surroundings effecting the vibrational frequencies. Further temperature dependent studies by the IR and Raman spectroscopy are under progress to explain this novel finding.

6. Conclusion

The temperature dependence and the polarization results and an improved resolution facilitated us to observe the extent of splitings of the bands due to low symmetry. Further splitting of these states due to the perturbation caused by spin-orbit coupling does not appear very clear in the region 13960–15600 cm^{-1}. Liehr and Ballhausen (1959) calculated the energies of spin-orbit split levels of $^3T_{1g}(^3F)$ excluding the symmetry effects, which gave a total splitting of 1260 cm^{-1}. Though this value appears to be comparable to the observed splitting of 1640 cm^{-1}, the low symmetry cannot be considered negligible. In fact, the polarization and temperature dependent studies on this complex revealed that, all the observed bands could be interpreted in terms of the splitting of the cubic levels due to tetragonal distortion alone as seen in the discussion. Hence a calculation including both the effects of spin-orbit coupling and distortion effects gives a better picture. This would give a total of 35 states. However, we limited ourselves to symmetry effects only since the observed spectrum did not resolve all the states.

Though all the observed polarizations of the transitions are consistent with the assignments, the intensity decrease of the transition at 8470 cm^{-1} as the temperature was lowered is not understandable since it has been assigned to an allowed transition. Its assignment is justified from polarization data and crystal field calculations. The observed temperature dependence of this band indicates that it gains intensity predominantly by vibronic mechanism than mixing of odd parity functions with d-orbitals of the metal ion. This may be an indication that the mixing of xy and $x^2 - y^2$ orbitals with odd parity functions is not considerable when compared to that of z^2 orbital in this complex. The considerable differences in calculated and observed energies of spin-forbidden transitions are due to the difficulty in identification of peak positions either by the overlap of neighbouring bands or insufficient resolution. A band deconvolution was not possible in this case due to too many shoulders and fine structure which makes it difficult to guess the number of component bands. A calculation of intensity ratios of the transitions $^3A_{2g} \rightarrow {}^3T_{1g}(F)$ and $^3A_{2g} \rightarrow {}^1E_g(D)$ which was carried out by Ballhausen and Liehr (1959) on $Ni(H_2O)^{2+}$ gave the ratio 4·3:0·1. Hence the assignment to the band at 13960 cm^{-1} given by Narayana *et al* (1968) as $^3A_{2g} \rightarrow {}^1E(^1D)$ may not be correct because of its large intensity. This conflict has been removed by our assignment to this band as $^3B_1 \rightarrow {}^3A_2[T_{1g}(F)]$. The temperature dependence and polarization data of this band and crystal field calculations completely agree with this assignment.

Acknowledgements

The financial support by the Department of Science and Technology, Delhi, India to carry out this work is gratefully acknowledged. The authors are also thankful to Dr G L Burkhart, Department of Chemistry, Navada University, for providing us with a FORTRAN program for deconvolution.

References

Balkanski M, Moch P and Shulman R G 1964 *J. Chem. Phys.* **40** 1897
Ballhausen C J and Liehr A D 1959 *Mol. Phys.* **2** 123

Ballhausen C J 1962 *Introduction to ligand field theory* (New York: McGraw-Hill)
Ballhausen C J 1971 *Spectroscopy in inorganic chemistry* (ed.) C N R Rao (New York: Academic Press) **1** 1
Barker B A and Fox M F 1980 *Chem. Soc. Rev.* **9** 143
Dingle R and Palmer R A 1966 *Theor. Chim. Acta* **6** 249
Holmes O G and McClure D S 1957 *J. Chem. Phys.* **26** 1686
Jorgensen C K 1955 *Acta Chim. Scand.* **9** 1362
Liehr A D and Ballhausen C J 1959 *Ann. Phys. (NY)* **6** 134
Muralikrishna C, Mahadevan C, Sastry S, Seshasayee M and Subramanian S 1983 *Acta Crystallogr.* **C39** 323
Narayana P A, Mehra A and Venkateswarlu P 1968 *Can. J. Phys.* **46** 1705
Pappalarado R 1957 *Nuovo Cimento* **6** 392
Perumareddi J R 1967 *Z. Naturforsch.* **B22** 908
Perumareddi J R 1972 *Z. Naturforsch.* **A27** 1820
Piper T S and Koertge N 1960 *J. Chem. Phys.* **32** 559
Van Niekerk J N and Schoening F R L 1953 *Acta Crystallogr.* **6** 609